Element-specific magnetic moments and spin-resolved density of states in CoFeMnZ (Z = Al, Ga; Si, Ge)

P. Klaer,[1,*] B. Balke,[2] V. Alijani,[2] J. Winterlik,[2] G. H. Fecher,[2] C. Felser,[2] and H. J. Elmers[1]

[1]*Institut für Physik, Johannes Gutenberg-Universität, D-55099 Mainz, Germany*

[2]*Institut für Anorganische Chemie und Analytische Chemie, Johannes Gutenberg-Universität Mainz, D-55099 Mainz, Germany*

(Received 8 July 2011; published 7 October 2011)

Using circular dichroism in x-ray-absorption spectroscopy (XAS/XMCD), we determined element-specific magnetic moments and spin-resolved unoccupied densities of states (DOS) for Co, Fe, and Mn in the quaternary Heusler compounds CoFeMnZ (Z = Al, Ga; Si, Ge). These compounds belong to a class of highly spin-polarized materials with cubic LiMgPdSn-type structure. Different structure models for the sublattice occupation leading to similar average magnetization values can be distinguished by comparison of element-specific moments with theory. We find that the compounds form similar structures, where Co, Fe, Mn, and Z occupy the X, X', Y, and Z sublattice of the related X_2YZ $L2_1$-Heusler structure, for which half-metallic behavior was predicted. The unoccupied partial DOS as derived from the XAS/XMCD spectra for Co, Fe, and Mn are compared to theoretical results. A good agreement is found for Co and Fe, while Mn spectra reveal additional final-state effects (multiplets).

DOI: 10.1103/PhysRevB.84.144413 PACS number(s): 71.20.−b, 75.47.−m, 75.50.Cc, 78.70.Dm

I. INTRODUCTION

Materials with high spin polarization have been intensively studied because of their potential use in spintronic applications.[1,2] Heusler alloys have been of particular interest because of their high Curie temperature and tunable electronic properties.[3–5] Recent years have seen an impressive increase of the tunneling magnetoresistance effect for devices using Heusler electrodes.[4,6–10] The tailoring of the band structure by partly replacing elements on the Y and Z site in the X_2YZ Heusler structure has been demonstrated both experimentally and theoretically.[11–16]

Quaternary compounds of the type $XX'YZ$ are a new class of materials with high potential in spintronic applications. The structure is derived from the Heusler structure by occupying the four interpenetrating fcc sublattices of the $L2_1$ structure with a different element. A prominent example is the quaternary compound CoFeMnSi, with a predicted half-metallic band structure.[17] However, three different structure types with different degrees of spin polarization may form that cannot be distinguished by standard x-ray diffraction because of similar scattering factors or by magnetometry because of the similar predicted magnetization values.[17]

We have used circular dichroism in x-ray-absorption spectroscopy (XAS/XMCD) for the determination of element-specific magnetic moments. As the element-specific moments considerably differ for different structure models, we unambiguously identify the LiMgPdSn-type I (space group $F\bar{4}3m$) as the correct structure type in the case of CoFeMnSi (see Fig. 1). For this particular structure, half-metallicity is predicted.[17] In this paper, experimental and theoretical results are compared for the four compounds CoFeMnZ (Z = Al, Ga; Si, Ge). From the XAS/XMCD data, we derived the element-specific partial density-of-states function (PDOS) for Co, Fe, and Mn using a previously described data evaluation.[13,18] The good agreement between theoretical and experimental results considering final-state effects confirms that the quaternary LiMgPdSn-type ferromagnets provide a class of promising materials for spintronic devices with high spin polarization.

II. EXPERIMENT

The polycrystalline samples were prepared by arc melting of stoichiometric quantities of the constituents in an argon atmosphere. Care was taken to avoid oxygen contamination. This was established by evaporation of Ti inside of the vacuum chamber before melting the compound, as well as additional purification of the process gas. The melting procedure was repeated three times to get a homogeneous material. After melting, the polycrystalline ingots were annealed in an evacuated quartz tube at 1073 K for two weeks. For powder investigations, a part of the sample was crushed by hand using a mortar.

The crystal structures of the samples were determined by x-ray diffraction (XRD) using Mo K_α radiation (Bruker D8 Advance). Details about the structure analysis of CoFeMnZ (Z = Al, Ga; Si, Ge) can be found in Ref. 19. CoFeMnSi shows a clear (110) and (200) reflection indicating a dominating type I structure. For CoFeMnAl, only the (200) reflection is observed, which is compatible with the dominating type I structure combined with a $B2$-type disorder. It is known for several years that Al-containing Heusler compounds are very susceptible to disorder effects.[12] The (200) fcc-superstructure reflections are absent or very small for CoFeMnGa and CoFeMnGe due to nearly equal scattering amplitudes of the constituting elements, which prevents a detailed structure analysis. Eventually, a distinction between the three proposed crystal structures is impossible because of the 3d constituents.

The magnetic properties were investigated by a superconducting quantum interference device (SQUID, Quantum Design MPMS-XL-5) using nearly punctual sample pieces of approximately 20 to 30 mg. Rods with dimensions $1 \times 1 \times 10$ mm^3 were cut from the ingots for spectroscopic investigations of the bulk samples.

X-ray-absorption spectroscopy (XAS) experiments were performed at the UE56/1-SGM beamline at the German synchrotron light source BESSY II. The samples were cleaved *in situ* in UHV ($p = 1 \times 10^{-9}$ Torr) directly before the measurement. An Au mesh monitored the incident photon flux. The

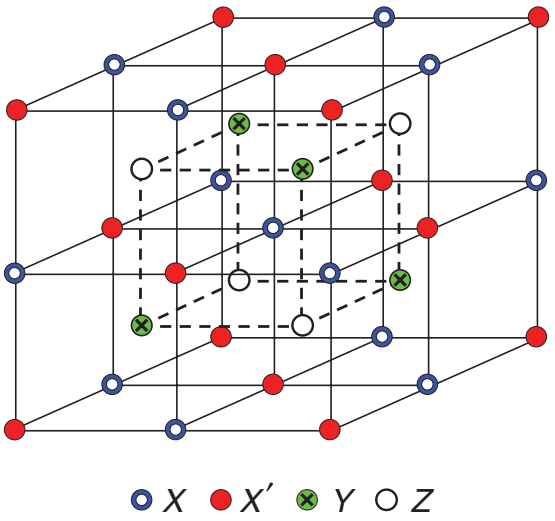

FIG. 1. (Color online) Cubic LiMgPdSn-type structure of the related X_2YZ $L2_1$-Heusler structure. Type I: Co, Fe, Mn, and Si atoms occupy the X, X', Y, and Z sublattice. Type II: Co, Mn, Fe, and Si occupy the X, X', Y, and Z sublattice. Type III: Fe, Mn, Co, and Si occupy the X, X', Y, and Z sublattice.

total electron yield served as a measure for the x-ray absorption signal. The sample was shielded by a conducting tube in order to collect all electrons. An external magnetic field of 1.22 T was applied along the direction of the incident x-ray beam, i.e., approximately perpendicular to the sample surface, and switched after each data point to determine the x-ray circular dichroism (XMCD) signal, while the polarization was kept constant. The energy resolution of the x-ray monochromator was set to 0.4 eV at 800 eV photon energy. An increase in the resolution to 0.1 eV at 800 eV for selected samples revealed only marginal changes in the observed spectra. This confirmed that the spectral shape is dominated by the intrinsic lifetime broadening of x-ray absorption. The XAS/XMCD measurements were performed at room temperature.

After these measurements a scanning electron microscope (SEM, Jeol JSM-6400) equipped with an energy dispersive x-ray spectroscopy (EDX) detection system was used to check the homogeneity and stoichiometry of the samples at the surface used for XAS/XMCD. An acceleration voltage of 20 kV and an inspection angle of 35° was set up. The quantitative data was corrected by the ZAF method, which relies on atomic number (Z), absorption (A), and fluorescence (F) effects. One should note that the accuracy of the determination of the relative atomic concentration is on the order of ±2 at.%. Within error limits, the relative atomic concentration in Table I

TABLE I. Relative atom concentrations given as atomic percentages of the samples for CoFeMnZ (Z = Al, Ga; Si, Ge) determined by an EDX analysis.

Z =	Co	Fe	Mn	Z
Al	24.4	25.3	25.0	25.3
Ga	24.3	26.4	24.6	24.7
Si	24.5	25.6	24.7	25.2
Ge	24.4	24.6	24.7	26.3

confirms the intended composition for the CoFeMnZ (Z = Al, Ga; Si, Ge) series. Element-specific EDX line scans confirm a homogeneous composition. In CoFeMnZ (Z = Ga, Si, Ge), we found small Mn and Fe clusters with an area fraction of one percent only.

III. COMPUTATIONAL DETAILS

The basic electronic-structure calculation and the optimization of the lattice parameter were carried out using the scalar-relativistic full potential linearized augmented plane-wave method as provided by WIEN2K.[20] The exchange-correlation functional was taken within the generalized gradient approximation (GGA) in the parametrization of Perdew, Burke, and Ernzerhof (PBE).[21] 816 k points in the irreducible wedge of the Brillouin zone of the primitive $F\,\bar{4}3m$ cell were used for integration. The number of plane waves was restricted by $R_{\mathrm{MT}} \cdot k_{\max} = 9$. Both total energy ($10^{-5}$ Ry) and charge ($10^{-2}\,e^-$) were used simultaneously as criteria for convergence. More description and electronic band-structure calculations can be found in Ref. 19.

For the disordered structures, further electronic-structure calculations have been carried out using the full relativistic spin-polarized Korringa-Kohn-Rostocker method (SPRKKR) provided by Ebert *et al.*[22–24] This program provides the coherent potential approximation (CPA) for calculating the properties of alloy systems with random distribution of the atoms. The SPRKKR calculations have been performed using the PBE generalized gradient approximation.[21] The CPA tolerance was set to 10^{-4} and the energy convergence criterion to 10^{-5}. f states were included in the basis of all atoms. 832 irreducible k points based on a $22 \times 22 \times 22$ mesh have been used for integration. The density of states is calculated for the double number of k points from the Green's function by adding a small imaginary part of 0.005 Ry to the energy. For smaller values, the band gaps may become better visible; however, at the same time, the DOS becomes much more noisy.

IV. X-RAY-ABSORPTION SPECTROSCOPY AND MAGNETIC MOMENTS

XAS/XMCD results are shown in Fig. 2 for the CoFeMnZ (Z = Al, Ga; Si, Ge) compounds measured at the Mn, Fe, and Co $L_{3,2}$edge. The XAS spectra were normalized at the postedge value, after subtracting a constant background from the raw data. The shape of the spectra appear pairwise similar for CoFeMnZ (Z = Al, Ga) and for CoFeMnZ (Z = Si, Ge). This is not surprising because the crystal structures are similar and the compounds with Al (Ga) and Si (Ge) are isoelectronic. Similar changes occur at the L_3 edge and L_2 edge.

The Co XAS spectra in Fig. 2(e) show for all samples a satellite peak A ($\sim$ 4 eV above L_3 maximum), which is indicative for a *sd*-band hybridization state similar to the related Co-based highly ordered Heusler compounds with a $L2_1$ crystal structure.[25,26] For Z = Ge, an additional satellite peak A' appears which was observed for the Co_2MnGe Heusler alloy, too.[13,27] A related satellite peak A is also visible for the Fe spectra for Z = Si, Ge [Fig. 2(c)]. We attribute the Fe peak A to a *sd*-band hybridization of Fe and the main group element Z = Si, Ge. As a consequence of the weaker hybridization

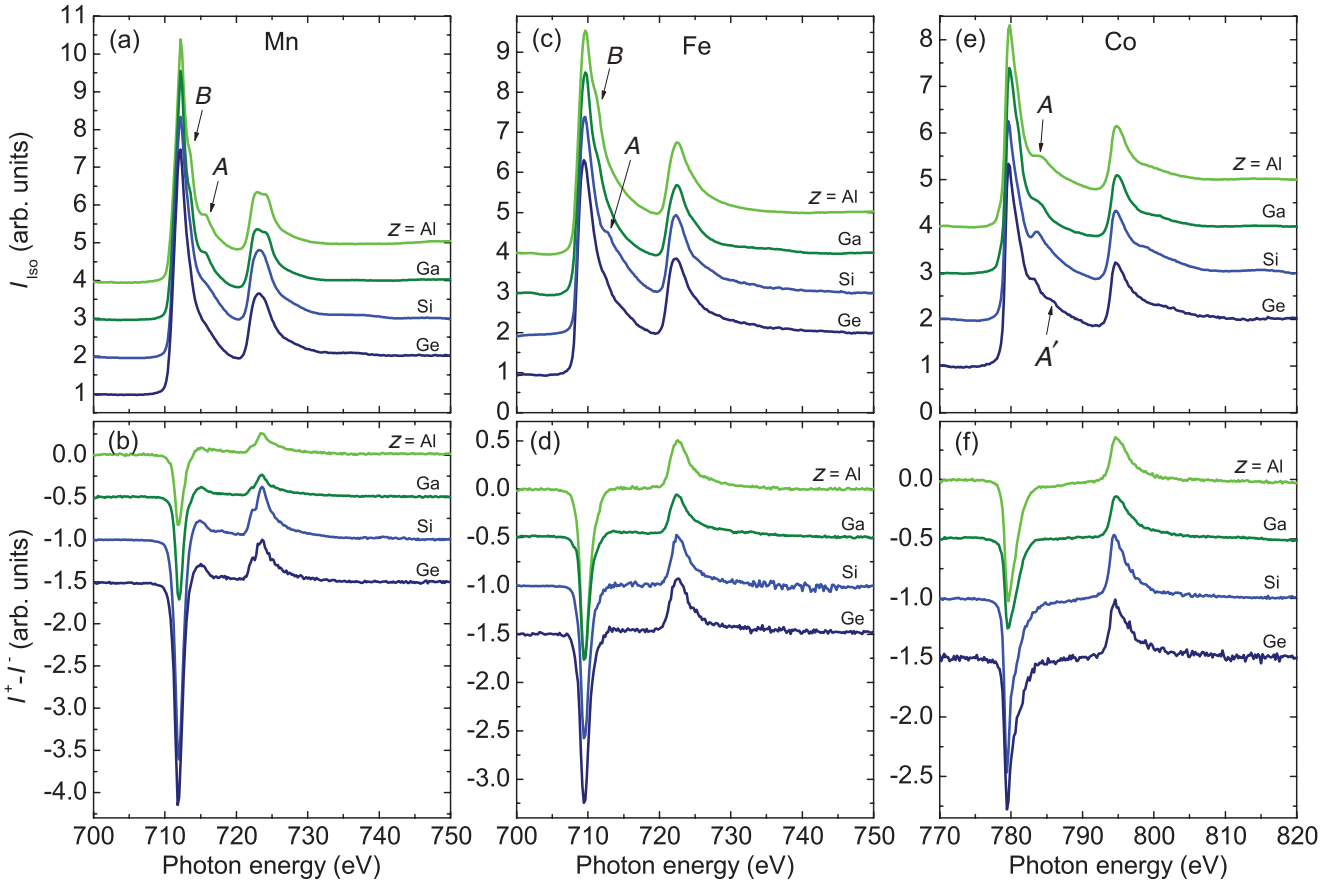

FIG. 2. (Color online) (a),(c),(e) X-ray absorption spectra for CoFeMnZ (Z = Al, Ga; Si, Ge) measured at the Mn, Fe, and Co $L_{3,2}$ edge averaged from total electron yield intensities I^+ and I^- for magnetization direction parallel and antiparallel to the x-ray polarization. (b),(d),(f) Corresponding XMCD spectra $I^+ - I^-$.

between Co/Fe and the main group element Z = Al, Ga the satellite peak A is broader for Co and absent in the Fe XAS spectra. $B2$ disorder (random occupation of the Mn and Z sublattice with these two elements) may lead to the loss of the hybridization peak.

CoFeMnZ (Z = Al, Ga) comprise two peaks indicated by A and B in the Mn spectra [Fig. 2(a)] and a peak B in the Fe spectra [Fig. 2(c)]. An explanation for peak A and peak B could be multiplet effects stemming from oxidation of Mn and Fe. However, an oxidation is unlikely as the sample was kept in UHV conditions after cleavage. No bulk contrast of oxygen was found in the EDX measurement. Instead, we attribute the Mn satellite peaks to a strong localization of Mn states and a corresponding by large contribution from multiplet effects caused by the configurational interaction of the core hole and the excited electron in the final state.[28] A similar effect has been observed in the case of Co_2MnZ (Z = Si, Al).[29]

The largest change with composition in the XMCD spectra occurs for Mn in Fig. 2(b). CoFeMnZ has for Z = Si, Ge larger asymmetries than that for Z = Al, Ga at the $L_{3,2}$ edge and a considerably more pronounced positive shoulder at 715 eV. The Fe and Co XMCD spectra in Figs. 2(d) and 2(f) show no significant changes with replacing the main group element Z. Only the maxima at the $L_{3,2}$ edge appear sharper for Z = Si, Ge.

From the element-specific XMCD spectra, we derived the magnetic spin moments μ_{spin} and the magnetic orbital moments μ_{orb} shown in Table II using the sum-rule analysis and assuming numbers of d holes N_h(Fe) = 3.4, N_h(Mn) = 4.5, and N_h(Co) = 2.5. For Mn, a jj-mixing correction factor c_{jj} = 1.5 was applied as described in Refs. 30 and 31.

TABLE II. Element-specific magnetic spin moments μ_{spin} and orbital moments μ_{orb} per atom for CoFeMnZ (Z = Al, Ga; Si, Ge) alloys as calculated from the sum rules and from first-principle GGA calculations are given in Bohr magnetons (μ_B).

Z =	μ	Co	Fe	Mn
Al	μ_{spin}	0.77 ± 0.02	0.91 ± 0.02	0.96 ± 0.02
	μ_{orb}	0.07 ± 0.01	0.07 ± 0.01	0.06 ± 0.01
	μ_{spin}^{GGA}	0.81	−0.13	2.44
Ga	μ_{spin}	0.85 ± 0.02	0.72 ± 0.02	1.05 ± 0.02
	μ_{orb}	0.03 ± 0.01	0.02 ± 0.01	0.09 ± 0.01
	μ_{spin}^{GGA}	0.77	−0.15	2.60
Si	μ_{spin}	0.88 ± 0.02	0.72 ± 0.02	2.22 ± 0.02
	μ_{orb}	0.06 ± 0.01	0.03 ± 0.01	0.09 ± 0.01
	μ_{spin}^{GGA}	0.88	0.52	2.70
Ge	μ_{spin}	0.82 ± 0.02	0.82 ± 0.02	1.95 ± 0.02
	μ_{orb}	0.06 ± 0.01	0.02 ± 0.01	0.04 ± 0.01
	μ_{spin}^{GGA}	0.86	0.50	2.71

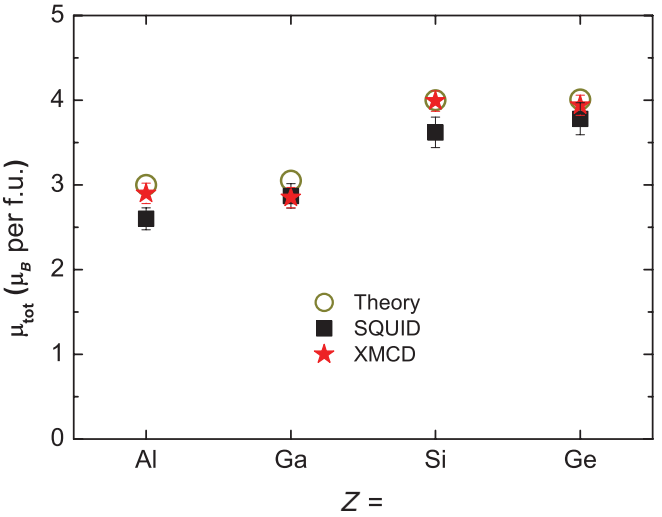

FIG. 3. (Color online) Total magnetic moments μ_{tot} for CoFeMnZ (Z = Al, Ga; Si, Ge) measured at RT with SQUID and XMCD. Theoretical magnetic moments are given for comparison.

The variation of Z in CoFeMnZ has no large impact on the Co and Fe magnetic moments (see Table II). In contrast, the increase in the valence electron number leads to a strong increase of the Mn magnetic moment. The replacing of the main group element Z = Al, Ga by the main group element Z = Si, Ge leads to a large increase in the Mn magnetic moment and the total magnetic moment by 1 μ_B per f.u. (see Fig. 3). The total magnetic moments resulting from XMCD are in good agreement with the measured SQUID results and the theoretical values.

In the case of Z = Si, Ge predictions from first principle GGA calculations assuming a perfect type I structure are in agreement with the experimentally determined element-specific magnetic moments. In contrast, these calculations predict an antiferromagnetically aligned Fe moment in the case of Z = Al, Ga which is not observed in the experiment. This indicates significant contributions from other structure types. Only in the case of Z = Si the structure analysis using XRD gives a closer hint on a prevailing type I structure with some contribution from type II. In order to quantify the disorder contribution, we present a detailed analysis of element-specific moments for the case of CoFeMnSi.

Table III compares the element-specific moments for CoFeMnSi with theoretical values from Ref. 17 for three different structure models. The structure models reflect a different occupation of the four sublattices in the LiMgPdSn-type structure with the four elements of the quaternary compound (see Fig. 1). For the type I structure, the Fermi level lies in an energy gap of 0.75 eV in the spin-down states (shown in Fig. 5). The electronic structure of the type II structure is similar to that of type I, but the Fermi level lies in a pseudogap. Therefore, the CoFeMnSi compound with type I or type II structure is a half-metallic or nearly half-metallic ferromagnet. The type III compound is a metallic ferromagnet with a large DOS value at E_F in the spin-down channel.

The sublattice occupation has a large effect on the size of the magnetic moments, in particular on the ratio of the Mn and Fe moment. The best agreement of the experimental and

TABLE III. Theoretical magnetic spin moments given in μ_B per atom (as labeled) for CoFeMnSi in the three nonequivalent superstructures from Ref. 17. Experimental magnetic spin moments μ_{spin} are given for comparison.

	μ_{Co}	μ_{Fe}	μ_{Mn}	μ_{Si}	μ_{tot}
Type I	0.878	0.576	2.649	−0.067	4.006
Type II	0.931	2.517	0.591	−0.010	3.959
Type III	1.786	1.804	1.898	−0.055	5.332
Expt.	0.88	0.72	2.22		3.82

theoretical results can be found for the type I structure in Table III. Structure type III can be excluded by comparing the theoretical and experimental Co magnetic moment and the total magnetic moment. The most indicative number for distinguishing between the type I and II structure models, which result in similar average magnetization values, is the ratio of Mn and Fe moments with predicted values of 4.60 (0.23) for model I (II). The experimental value of 3.08 is close to the value of model I. In the following, we assume that disorder involves exclusively structure type I and II with the Mn and Fe moments as given in Table III. With the volume fraction r for structure type I, one obtains average Mn (Fe) moments,

$$\bar{\mu}_i = r \cdot \mu_i^{\mathrm{I}} + (1-r) \cdot \mu_i^{\mathrm{II}}, \quad i = \mathrm{Mn,Fe}. \tag{1}$$

The ratio of the averaged Mn and Fe magnetic moments,

$$\frac{\bar{\mu}_{\mathrm{Mn}}}{\bar{\mu}_{\mathrm{Fe}}} = \frac{r \cdot \mu_{\mathrm{Mn}}^{\mathrm{I}} + (1-r) \cdot \mu_{\mathrm{Mn}}^{\mathrm{II}}}{r \cdot \mu_{\mathrm{Fe}}^{\mathrm{I}} + (1-r) \cdot \mu_{\mathrm{Mn}}^{\mathrm{II}}}, \tag{2}$$

must equal the experimental value of 3.08. From the equation, we obtain a volume fraction r = 0.89, indicating a disorder on the order of 11%.

An alternative approach is a direct comparison of theoretical calculated moments for various types of disorder with the experimental data. The disorder cannot be varied continuously but a large unit cell can be used.[32] The result is shown in Fig. 4. The total magnetization is nearly independent on the contribution of the type II structure (x). The Fe moment

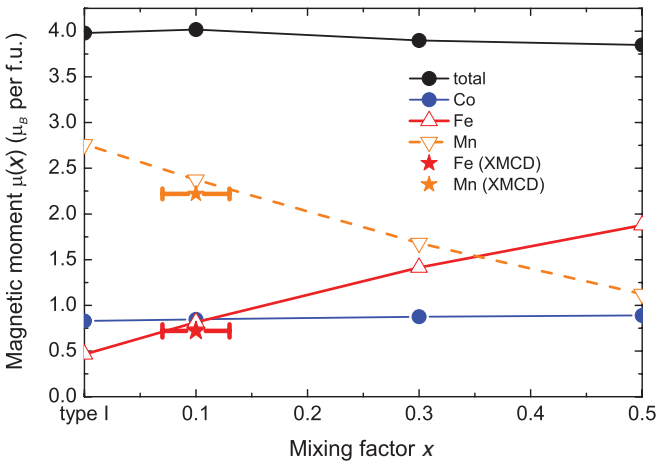

FIG. 4. (Color online) Theoretical calculated magnetic moments for CoFeMnSi depending on the contribution of the type II structure (x) compared with the XMCD results.

increases and the Mn moment decreases with increasing x. A comparison with the experimental data indicates a contribution of $x = 0.1$, in good agreement with the analytical discussion above.

V. ELEMENT-SPECIFIC AND SPIN-RESOLVED UNOCCUPIED DENSITY OF STATES

The self-consistent electronic-structure calculation of the partial density of states (PDOS) for the type I CoFeMnSi structure (Fig. 5) shows that the lower boundary of the minority band gap near E_F is given by the Co and Fe states. Therefore, an experimental determination of the element-specific Co, Fe, and Mn density of states is essential. CoFeMnZ (Z = Al, Ga; Si, Ge) compounds exhibit a calculated electronic structure, which is typical for a fully spin-polarized half-metallic ferromagnetic Heusler compound (see also Fig. 6).

Experimental data for the spin-resolved unoccupied Co, Fe, and Mn PDOS is shown in Fig. 6 as derived from the corresponding L_3-edge XAS/XMCD data. For the calculation, we used the spin-resolved unoccupied PDOS function following from the XAS spectra I^+ and I^-,

$$D^{\uparrow(\downarrow)}(1 - f_F) \propto I_{\text{iso}} - s + (-)\frac{1}{P_j}\frac{I^+ - I^-}{2}, \qquad (3)$$

where f_F denotes the Fermi function, I_{iso} denotes the isotropic absorption coefficient $(I^+ + I^-)/2$, s is the step function, and P_j is the spin polarization of the excited photoelectrons, i.e., $P_{L3} = 0.25$ and $P_{L2} = -0.5$. This procedure has been applied before to the case of Co in Co_2YZ Heusler alloys (Refs. 13, 16, and 18). In this case, an electron correlation effect causes a shift of the majority PDOS of $\Delta E_c = 0.5$ eV with respect to the minority states for the Co data. The position of the Fermi level was derived from the initial increase in the majority states considering the energy shift of ΔE_c. Recently, a direct comparison of XAS/XMCD spectra with calculations confirmed the existence of this electron correlation effect for Co_2TiSn.[33]

For Mn and Fe, the value for ΔE_c is set to zero. The Mn and Fe majority PDOS comprises localized states at E_F both for majority and minority states in contrast to the Co PDOS. Because of the lifetime broadening of the XAS spectra, we have deconvoluted the experimental spectra with a Lorentzian function with a width of $\Gamma = 0.35$ eV.

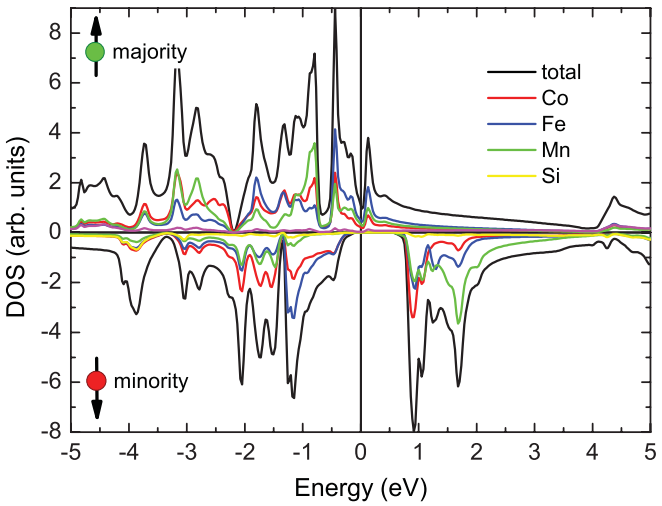

FIG. 5. (Color online) Spin-resolved PDOS for CoFeMnSi using *ab initio* calculations according to Ref. 17.

For all three elements in CoFeMnZ (Z = Si, Ge), the comparison of theoretical and experimental results for the minority PDOS reveals a fair agreement considering lifetime broadening (Fig. 6). In particular, the PDOS minority maxima agree well. This observation confirms the assumption of $\Delta E_c = 0.5$ eV in the case of Co and $\Delta E_c = 0$ eV in the case of Fe and Mn. The same values of ΔE_c were assumed in the case of Z = Al, Ga. The agreement is similarly good for CoFeMnGe. In the case of Z = Al, Ga, the experimental minority PDOS for Fe and Co are shifted to somewhat larger energies compared to theoretical values. This might be attributed to a residual $B2$ disorder in these compounds, as also observed by x-ray diffraction.

As expected from the XAS spectra, the unoccupied PDOS shown in Fig. 6 of the isoelectronic compounds Z = Al, Ga and Z = Si, Ge behave pairwise similarly. The increase in the Co minority PDOS shows a steeper slope than the Fe and Mn minority PDOS. The smaller slope in the Mn PDOS fits well with theoretical GGA calculations showing a much broader feature of 1.5 eV width for Mn compared to 0.2 eV in the case of Co.

The experimental majority Co PDOS shows a flat line, except for a small peak near 1 eV above E_F, expected from theoretical calculations. In contrast, the Fe and even more the Mn majority PDOS reveal a rich structure that has no correspondence in the theoretical majority PDOS. A prominent difference between the Co PDOS and the Mn, and Fe PDOS is the stronger localization of electronic states in the latter case (see below), according to calculations. These localized states lead to multiplet effects splitting a single transition into a number of absorption peaks. For the case of Mn in Co_2MnSi and Rh_2MnSi, this has been explicitly shown by comparison to an atomic model.[28,34] Therefore, we attribute the rich structure of the majority Fe and Mn PDOS to the occurrence of these multiplet effects. The ground-state GGA calculations do not consider these final-state effects, and hence it is no surprise that theory and experiment do not agree in this case. Although not obvious, these multiplet effects might also alter the minority PDOS and an interpretation of the Mn and Fe PDOS has to be done with care.

The difference between the energy position of the minority maximum and the Fermi energy $\Delta E_X = E^X_{v,\max} - E_F$ (X = Mn, Fe, and Co) depends on Z as summarized in Fig. 7. Assuming a rigid-band model, the replacing of Z = Al, Ga by Z = Si, Ge shifts the Fermi energy from the minority band gap in the Co, Fe, and Mn PDOS spectra toward the conduction band edge. The additional valence electron fills majority states at the Fermi energy. According to the rigid-band model, one would expect that the shift of the Fermi energy increases with decreasing majority PDOS at E_F. The Co PDOS shows the smallest value at E_F, and the observed change of ΔE_X from main group element III (Z = Al, Ga) to group IV (Z = Si, Ge) is largest for Co. Therefore, our experimental observation is in agreement with the rigid-band model. In contrast, the theoretical calculations show no significant changes of ΔE_X with changing Z. The GGA calculations show a large increase

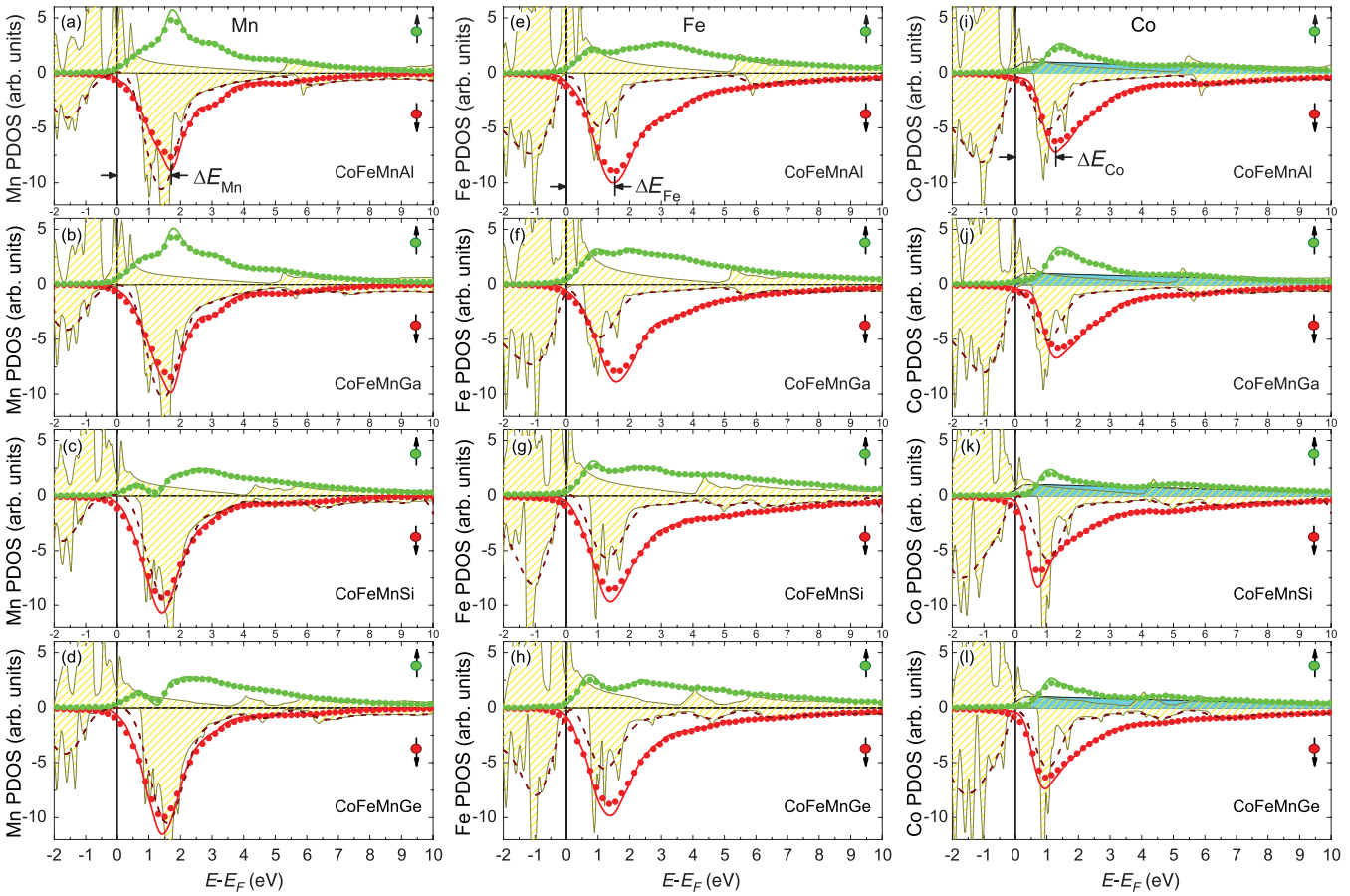

FIG. 6. (Color online) Spin-resolved PDOS calculated from the XAS/XMCD data (dots) measured at the L_3 edge for CoFeMnZ (Z = Al, Ga; Si, Ge) samples as indicated in the figure. Full lines show the deconvoluted data. Data from theoretical *ab initio* calculations are indicated by a yellow patterned area. The dashed lines show the smoothened theoretical data of the minority PDOS. Full filled areas indicate the function used for approximation of the Co itinerant band as measured [blue (dark)] and shifted by ΔE_c [light blue (gray)].

in minority states at 1 eV above E_F for all elements. In the case of Co, the minority maximum increases with respect to the second maximum at 1.7 eV for replacing Al by Si. Considering lifetime broadening, this feature leads to a shift. We have smoothened the theoretical PDOS for considering dynamic correlation effects (see Fig. 6). The minority maxima resulting from this procedure fit considerably better to the experimental values as indicated in Fig. 7.

Pronounced discrepancies still remain for the case of Z = Al, Ga with a systematically larger experimental value of ΔE_X compared to theory. A possible reason is the occurrence of $B2$ disorder in this case, while theory considers a perfectly ordered atomic structure. However, a previous study on epitaxial films revealed a decrease of ΔE_{Co} instead of an increase with an increase in disorder for $Co_2Fe(Al_{1-x}Si_x)$.[18]

VI. SUMMARY

We present element-specific magnetic moments and the element-specific spin-resolved DOS of the quaternary CoFeMnZ (Z = Al, Ga; Si, Ge) alloy using XMCD. A comparison of calculated moments with the evaluated Co, Fe, and Mn magnetic moments clearly allows one to distinguish between various structure models confirming the proposed LiMgPdSn-type structure in the case of Z = Si with predicted half-metallicity from Refs. 17 and 19. Exchange of the main group element from group III (Z = Al, Ga) by those from

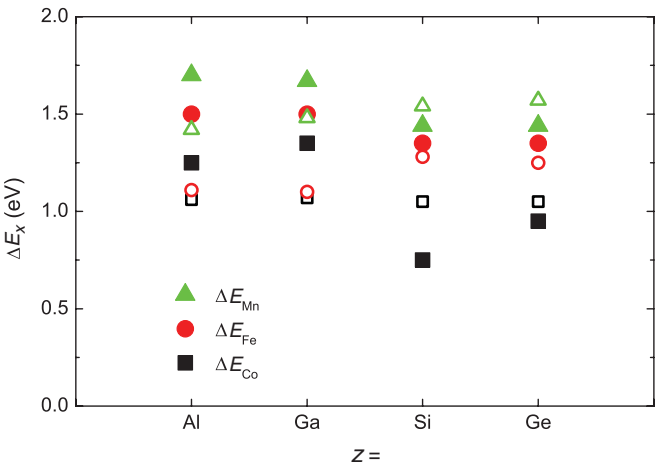

FIG. 7. (Color online) Element-specific values for ΔE_X (X = Mn, Fe, and Co) as defined in Fig. 6 for CoFeMnZ (Z = Al, Ga; Si, Ge). Theoretical values are denoted for comparison with open symbols.

group IV (Z = Si, Ge) causes an increase in the Mn magnetic moment of 1 μ_B per formula unit. From XAS/XMCD, we derived the element-specific spin-resolved unoccupied density of states for Co, Fe, and Mn, which can be directly compared to *ab initio* GGA calculations. We find a shift of the spectral weight with replacing the Z = Al, Ga main group element by Z = Si, Ge explained by the rigid-band model similar to the case of $Co_2Mn(Ga_{1-x}Ge_x)$.[13] The largest shift of the Fermi energy with respect to the half-metallic band gap is observed for the Co PDOS due to the small density of states in the majority band. Therefore, with an improved sample preparation, a design of a half-metallic ferromagnet with CoFeMnZ (Z = Si and, especially, Z = Ge) seems to be possible.

ACKNOWLEDGMENTS

The authors are thankful for financial support from the DFG (Grant No. FOR 559) and BMBF (Grant No. ES3XBA/5) and S. Cramm for support at BESSY.

*klaer@uni-mainz.de

[1] C. Felser, G. H. Fecher, and B. Balke, Ang. Chem. Int. Ed. **46**, 668 (2007).
[2] H. Ohno, Nat. Mater. **9**, 952 (2010).
[3] J. Kübler, G. H. Fecher, and C. Felser, Phys. Rev. B **76**, 024414 (2007).
[4] W. Wang, H. Sukegawa, R. Shan, S. Mitani, and K. Inomata, Appl. Phys. Lett. **95**, 182502 (2009).
[5] K. Özdogan, B. Aktas, I. Galanakis, and E. Sasioglu, J. Appl. Phys. **101**, 073910 (2007).
[6] S. Kämmerer, A. Thomas, A. Hütten, and G. Reiss, Appl. Phys. Lett. **85**, 79 (2004).
[7] M. Yamamoto, T. Marukame, T. Ishikawa, K. Matsuda, T. Uemura, and M. Arita, J. Phys. D **39**, 824 (2006).
[8] Y. Sakuraba, M. Hattori, M. Oogane, Y. Ando, H. Kato, A. Sakuma, T. Miyazaki, and H. Kubota, Appl. Phys. Lett. **88**, 192508 (2006).
[9] N. Tezuka, N. Ikeda, S. Sugimoto, and K. Inomata, Jpn. J. Appl. Phys. **46**, L454 (2007).
[10] K. Inomata, N. Ikeda, N. Tezuka, R. Goto, S. S. M. Wojcik, and E. Jedryka, Sci. Technol. Adv. Mater. **9**, 014101 (2008).
[11] G. H. Fecher, B. Balke, S. Ouardi, C. Felser, G. Schönhense, E. Ikenaga, J.-J. Kim, S. Ueda, and K. Kobayashi, J. Phys. D **40**, 1576 (2007).
[12] B. Balke, S. Wurmehl, G. H. Fecher, C. Felser, and J. Kübler, Sci. Technol. Adv. Mater. **9**, 014102 (2008).
[13] P. Klaer, M. Kallmayer, C. G. F. Blum, T. Graf, J. Barth, B. Balke, G. H. Fecher, C. Felser, and H. J. Elmers, Phys. Rev. B **80**, 144405 (2009).
[14] B. S. D. C. S. Varaprasad, A. Rajanikanth, Y. K. Takahashi, and K. Hono, Appl. Phys. Express **3**, 023002 (2010).
[15] Y. Sakuraba, K. Takanashi, Y. Kota, T. Kubota, M. Oogane, A. Sakuma, and Y. Ando, Phys. Rev. B **81**, 144422 (2010).
[16] P. Klaer, T. Bos, M. Kallmayer, C. G. F. Blum, T. Graf, J. Barth, B. Balke, G. H. Fecher, C. Felser, and H. J. Elmers, Phys. Rev. B **82**, 104410 (2010).
[17] X. Dai, G. Liu, G. H. Fecher, C. Felser, Y. Li, and H. Liu, J. Appl. Phys. **105**, 07E901 (2009).
[18] M. Kallmayer, P. Klaer, H. Schneider, E. ArbeloJorge, C. Herbort, G. Jakob, M. Jourdan, and H. J. Elmers, Phys. Rev. B **80**, 020406(R) (2009).
[19] V. Alijani, S. Ouardi, G. H. Fecher, J. Winterlik, S. S. Naghvi, X. Kozina, G. Stryganyuk, C. Felser, E. Ikenaga, Y. Yomashita, S. Ueda, and K. Kobayashi (unpublished).
[20] P. Blaha, K. Schwarz, G. K. H. Madsen, D. Kvasnicka, and J. Luitz, WIEN2k, An Augmented Plane Wave + Local Orbitals Program for Calculating Crystal Properties (Karlheinz Schwarz, Techn. Universitaet Wien, Wien, Austria, 2001).
[21] J. P. Perdew, K. Burke, and M. Ernzerhof, Phys. Rev. Lett. **77**, 3865 (1996).
[22] H. Ebert, in *Electronic Structure and Physical Properties of Solids*, Lecture Notes in Physics Vol. 535, edited by H. Dreyssé (Springer, Berlin, 2000); H. Ebert *et al.*, The MUNICH SPR-KKR package, version 3.6, [http://olymp.cup.uni-muenchen.de/ak/ebert/SPRKKR].
[23] H. Ebert, in *Electronic Structure and Physical Properties of Solids. The Use of the LMTO Method*, Lecture Notes in Physics Vol. 535, edited by H. Dreysee (Springer-Verlag, Berlin, Heidelberg, 1999), p. 191.
[24] H. Ebert, J. Minár, and V. Popescu, in *Band-Ferromagnetism*, Lecture Notes in Physics Vol. 580, edited by K. Baberschke, M. Donath, and W. Nolting (Springer-Verlag, Berlin, Heidelberg, 2001), p. 371.
[25] N. D. Telling, P. S. Keatley, G. van der Laan, R. J. Hicken, E. Arenholz, Y. Sakuraba, M. Oogane, Y. Ando, and T. Miyazaki, Phys. Rev. B **74**, 224439 (2006).
[26] H. J. Elmers, G. H. Fecher, D. Valdaitsev, S. A. Nepijko, A. Gloskovskii, G. Jakob, G. Schönhense, S. Wurmehl, T. Block, C. Felser, P. C. Hsu, W. L. Tsai, and S. Cramm, Phys. Rev. B **67**, 104412 (2003).
[27] J. Grabis, A. Bergmann, A. Nefedov, K. Westerholt, and H. Zabel, Phys. Rev. B **72**, 024437 (2005).
[28] F. de Groot, Coord. Chem. Rev. **249**, 31 (2005).
[29] N. D. Telling, P. S. Keatley, G. van der Laan, R. J. Hicken, E. Arenholz, Y. Sakuraba, M. Oogane, Y. Ando, K. Takanashi, A. Sakuma, and T. Miyazaki, Phys. Rev. B **78**, 184438 (2008).
[30] E. Goering, Philos. Mag. **85**, 2895 (2005).
[31] A. Scherz, H. Wende, C. Sorg, K. Baberschke, J. Minár, D. Benea, and H. Ebert, Phys. Scr., T **115**, 586 (2005).
[32] V. Jung, G. H. Fecher, B. Balke, V. Ksenofontov, and C. Felser, J. Phys. D **42**, 084007 (2009).
[33] M. Meinert, J. Schmalhorst, H. Wulfmeier, G. Reiss, E. Arenholz, T. Graf, and C. Felser, Phys. Rev. B **83**, 064412 (2011).
[34] P. Klaer, M. Kallmayer, H. J. Elmers, L. Basit, J. Thöne, S. Chadov, and C. Felser, J. Phys. D **42**, 084001 (2009).